Enhanced Oxygen Transfer Rate of Chemical Looping Combustion through Lattice Expansion on $CuMn_2O_4$ Oxygen Carrier

Boseok Seo[1], Jimin Lyu[2], Namgyu Son[3], Misook Kang[3], No-Kuk Park[4], Seung Jong Lee[5], Jin Wook Lee[5], Yongseung Yun[5], Ho-Jung Ryu[6], Jeom-In Baek[7], Dohyung Kang*[,2], Minkyu Kim*[,1]

[1]School of Chemical Engineering, Yeungnam University, 280 Daehak-ro, Gyeongsan, Gyeongbuk, 38541, Korea

[2]Department of Future Energy Convergence, Seoul National University of Science and Technology, 232 Gongneung-Ro, Nowon-Gu, Seoul 01811, Republic of Korea

[3]Department of Chemistry, College of Natural Sciences, Yeungnam University, Gyeongsan, Gyeongbuk 38541, Republic of Korea

[4]Institute of Clean Technology, Yeungnam University, 280 Daehak-ro, Gyeongsan, Gyeongbuk, 38541, Korea

[5]Institute for Advanced Engineering, 175-28, Goan-ro 51 beon-gil, Baegam-myeon, Cheoin-gu, Yongin-si, Gyeonggi-do, 17180, Korea

[6]Korea Institute of Energy Research, 152 Gajeong-ro, Yuseong-gu, Daejeon, 34129, Republic of Korea

[7]Korea Electric Power Corporation Research Institute, 105 Munji-ro, Yuseong-gu, Daejeon, 34056, Republic of Korea

*To whom correspondence should be addressed, dkang@seoultech.ac.kr (D.K) and mk_kim@ynu.ac.kr (M.K)

S1. NEB images of CH4 oxidation reaction

The NEB images of initial (IS), transition (TS) and final (FS) states corresponding to the results in figure 2 are provided in the figure S1.

a) $CH_4^* + O^* \rightarrow CH_3^* + OH^*$		
IS	TS	FS
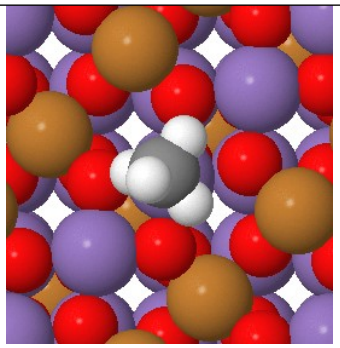	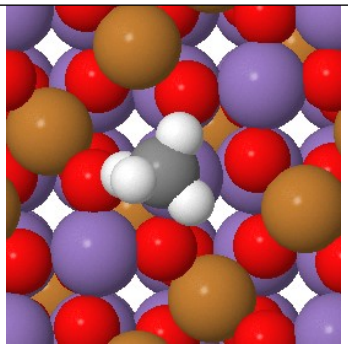	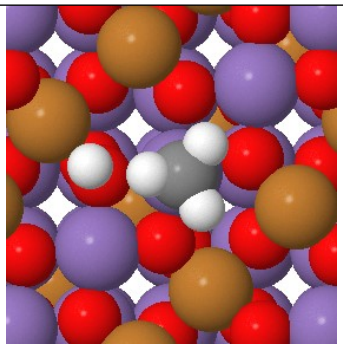
b) $CH_3^* + O^* \rightarrow CH_3O^*$		
IS	TS	FS
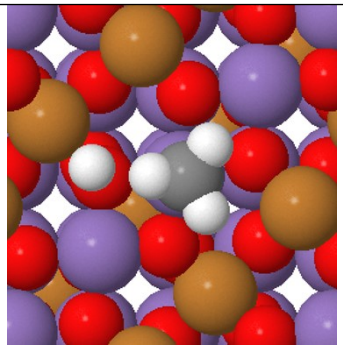	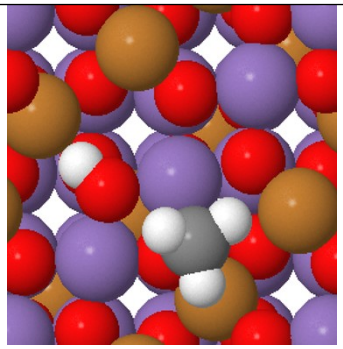	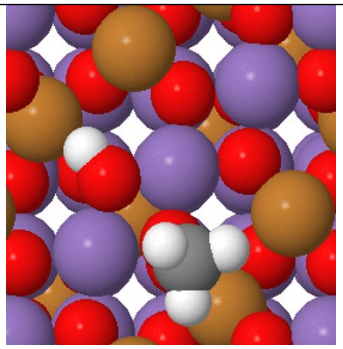
c) $CH_3O^* + O^* \rightarrow CH_2O^* + OH^*$		
IS	TS	FS
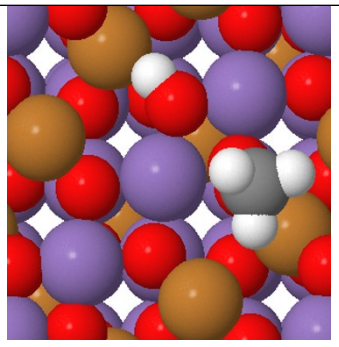	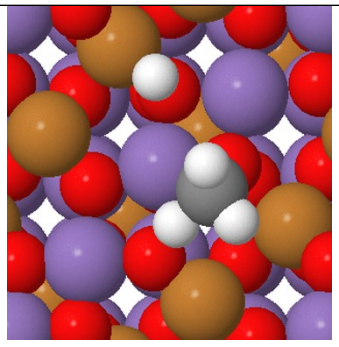	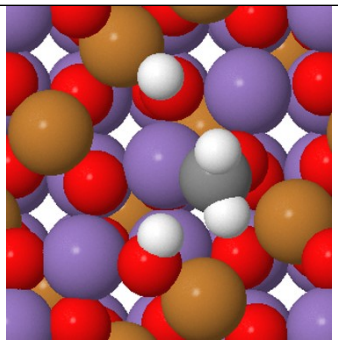
d) $CH_2O^* + O \rightarrow CHO^* + OH^*$		
IS	TS	FS

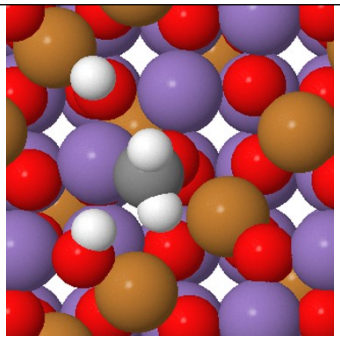
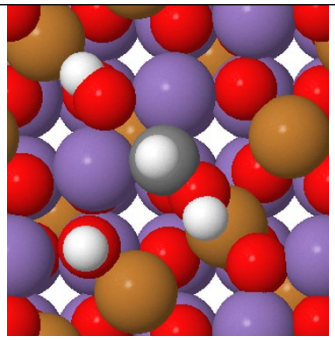
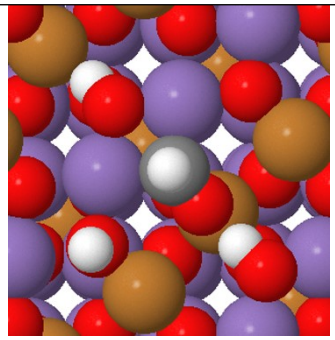

e) CHO* + O*→ CO* + OH*

IS	TS	FS

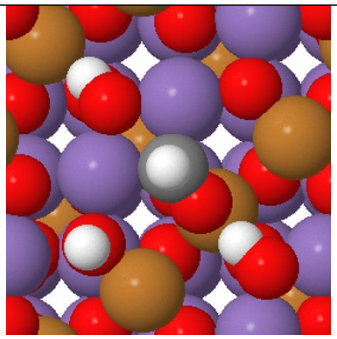
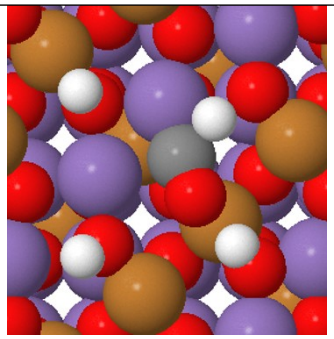
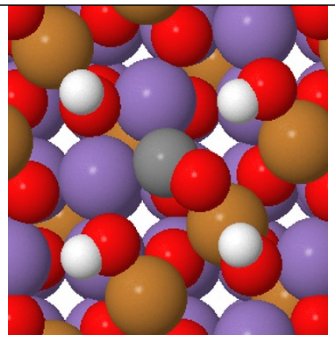

Figure S1. NEB images of IS, TS, and FS for CH4 oxidation reactions on S-$CuMn_2O_{4-x}$ (50% lattice expanded). The corresponding energy barriers are provided in the figure 2.

S2. SEM and BET results

The morphology of $CuMn_2O_4$ and S-$CuMn_2O_{4-x}$ particles are observed in the scanning electron microscopy (SEM) images presented in Figure S2. The porosity of $CuMn_2O_4$ and S-$CuMn_2O_{4-x}$ particles measured through N_2 adsorption-desorption isotherms are displayed in Figure S3. There is no discernible difference observed between morphology and porosity of two particle types.

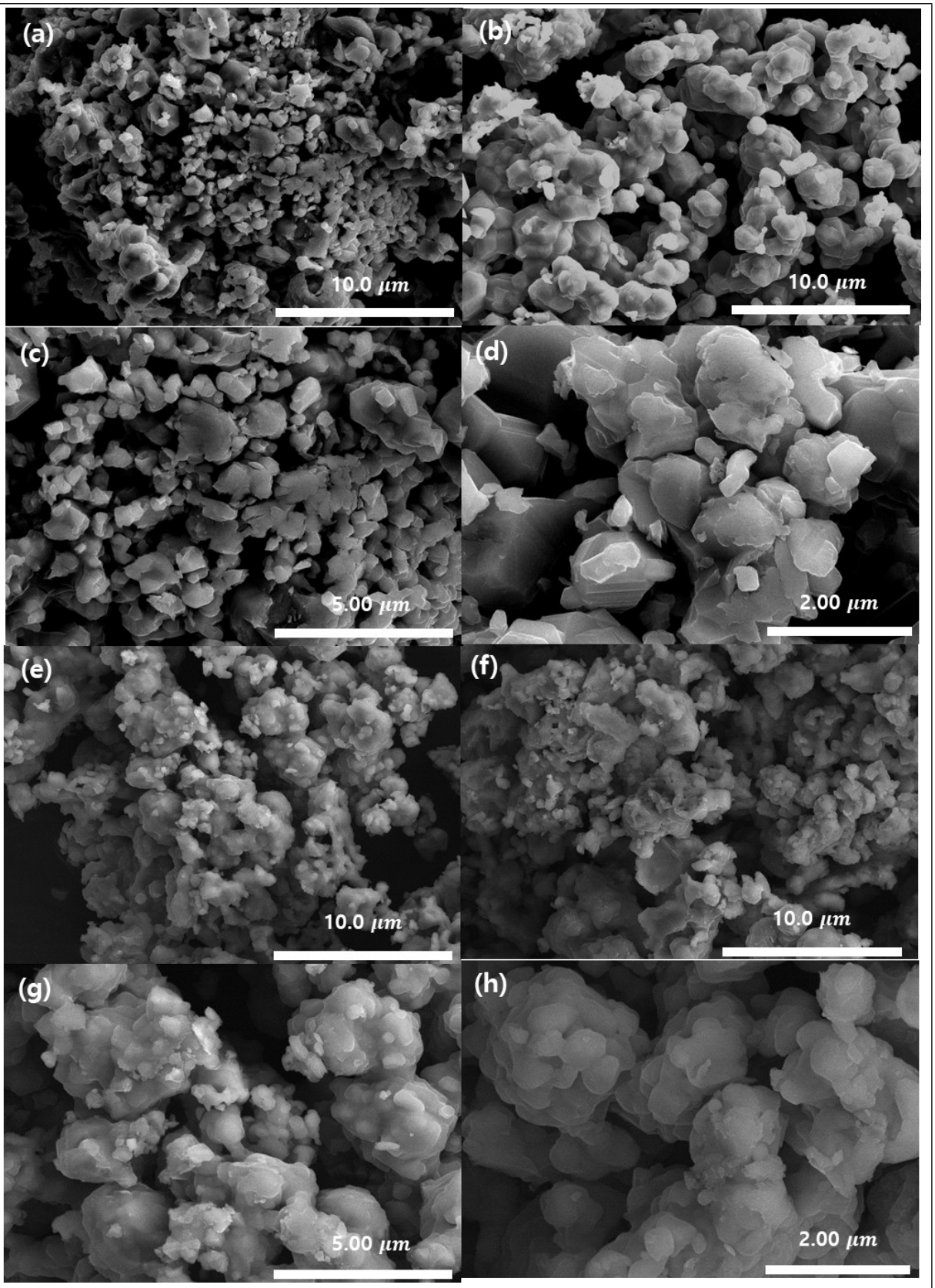

Figure S2. SEM images of $CuMn_2O_4$ (a, b, c, d) and S-$CuMn_2O_{4-x}$ (e, f, g, h) with different scales.

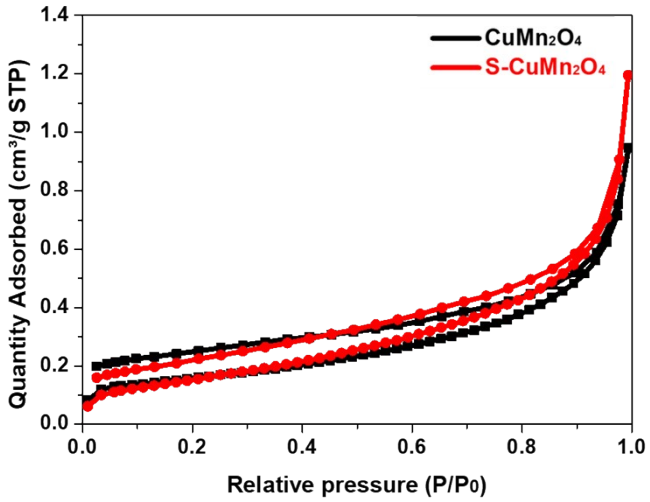

Figure S3. N_2 adsorption-desorption isotherms of $CuMn_2O_4$ (black line) and S-$CuMn_2O_{4-x}$ (red line)

S3. Stability analysis for lattice expanded $CuMn_2O_4$

We investigated the impact of lattice expansion on the stability of the $CuMn_2O_4$ structure by assessing the variation in DFT energy with respect to lattice parameters, as depicted in Figure S4. The DFT energy of the pristine $CuMn_2O_4$ (corresponding to 0% lattice expansion) was established as the reference energy, set to 0 eV, as this lattice constant represents the most stable configuration for $CuMn_2O_4$. In this context, it is important to note that a more positive energy value indicates a lower structural stability. The simulations revealed that, as the lattice undergoes expansion, the DFT energy increases, signifying a decrease in the structural stability. In simpler terms, maintaining the lattice-expanded structure without the presence of substituted larger atom proves to be non-trivial. These results strongly corroborate the experimental observation of residual sulfur in lattice-expanded $CuMn_2O_4$ (S-$CuMn_2O_{4-x}$).

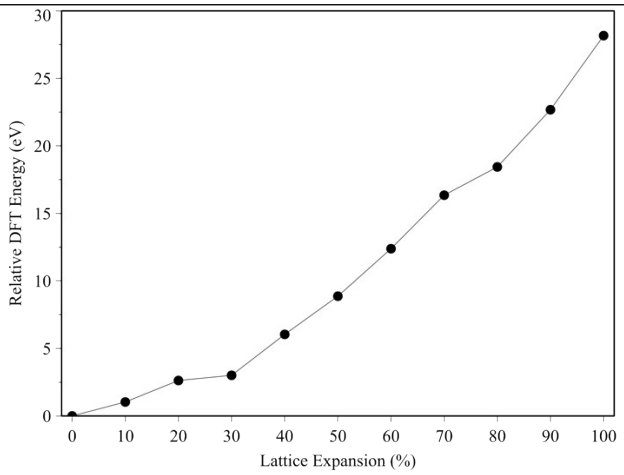

Figure S4. Energy diagram of relative DFT energy varying with lattice expansion. The DFT energy of the pristine $CuMn_2O_4$ (corresponding to 0% lattice expansion) was established as the reference energy, set to 0 eV